Asymmetric Hydrogenation of Methyl-(Z)-α-acetamidocinnamate Catalyzed by {1,2-Bis((phenyl-ō-anisoyl)phosphino)ethane}rhodium(I): Kinetics, Mechanism, and Origin of Enantioselection

Clark R. Landis and Jack Halpern*

Contribution from the Department of Chemistry, The University of Chicago, Chicago, Illinois 60637. *Received August 5, 1986*

Abstract: The following aspects of the hydrogenation of methyl-(Z)-α-acetamidocinnamate (mac), catalyzed by {R,R-1,2-bis((phenyl-o-anisoyl)phosphino)ethane}rhodium(I), $[Rh(dipamp)]^+$, have been examined: (1) thermodynamics and kinetics of the formation of the two diastereomeric $[Rh(dipamp)(mac)]^+$ adducts, (2) kinetics of the reaction of the major adduct with H_2, (3) kinetics and enantioselectivity of the overall catalytic hydrogenation reaction, and (4) the influence of temperature and H_2 pressure on the rate and enantioselectivity. It is concluded that the predominant product enantiomer, (S)-N-acetylphenylalanine methyl ester, is derived from the minor (less stable) $[Rh(dipamp)(mac)]^+$ adduct by virtue of its much higher reactivity toward H_2. Kinetic parameters for the several component steps of the catalytic cycle are evaluated. The inverse dependence of the optical yield on the H_2 partial pressure is shown to be due to trapping of the $[Rh(dipamp)(mac)]^+$ adducts by reaction with H_2 and, thus, inhibiting their diastereomeric interconversion. This effect can be offset by increasing temperature.

The asymmetric catalytic hydrogenation of prochiral olefins constitutes one of the most impressive achievements to date in catalytic selectivity.[1] By using cationic rhodium complexes containing chiral chelating diphosphine ligands, in combination with substrates such as methyl-(Z)-α-acetamidocinnamate (mac, **A**), optical yields (>99% enantiomeric excess) and rates have been achieved that rival those of enzymic catalysts.[1]

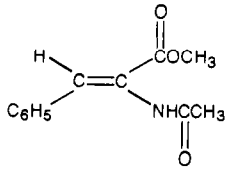

MAC (A)

Our earlier studies on the hydrogenation of mac using an achiral model catalyst, $[Rh(diphos)S_2]^+$, (diphos = 1,2-bis(diphenylphosphino)ethane, **B**; S = methanol), derived by in situ hydrogenation of $[Rh(diphos)(nbd)]^+$ (nbd = norbornadiene), have led to elucidation of the mechanism described by Figure 1.[2] Species **1**, **2**, and **4** have been characterized by NMR, and the adduct **2** also crystallographically.[2]

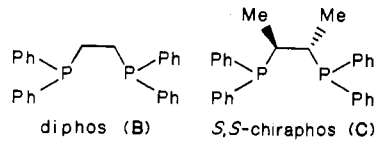

diphos (B) S,S-chiraphos (C)

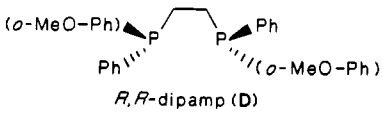

R,R-dipamp (D)

As depicted in Figure 1, mac is coordinated to the rhodium atom in the adduct **2** as a chelating ligand, through the C=C bond as well as through the oxygen atom of the amide group. Under ambient conditions the formation of **2** is rapid, and the equilibrium (**1** ⇌ **2**) is displaced far to the right ($K_1^{eq} = k_1/k_{-1} \sim 10^4\ M^{-1}$), so that the oxidative addition of H_2 (**2** → **3**) is the turnover-limiting step of the catalytic cycle. At low temperatures (< −40 °C) the product-forming reductive elimination step (**4** → **1**) becomes turnover-limiting so that the alkyl hydride intermediate **4** accumulates and can be intercepted and characterized.[2c]

When the mechanism is extended to catalysts containing chiral phosphine ligands such as chiraphos (**C**) or dipamp (**D**), it must be modified, in accord with Figure 2, to accommodate the formation of diastereomeric forms of **2** and of the subsequent reaction intermediates. (In this scheme, and subsequently in this paper, the superscripts maj and min are used to designate the manifolds arising from the major (i.e., thermodynamically more stable) and minor diastereomers of the $[Rh(diphosphine)(mac)]^+$ adduct.) Whereas the binding step (**1** ⇌ **2**) is reversible, the available evidence suggests that the subsequent steps, i.e., oxidative addition of H_2 to **2** (**2** → **3**), migratory insertion of the C=C bond into the Rh–H bond (**3** → **4**), and reductive elimination of the product (**4** → **1**) are irreversible.[3] Thus, as the first irreversible step in the catalytic cycle, the oxidative addition of H_2 (**2** → **3**) dictates the enantioselection.

Previously, we have investigated the hydrogenation of ethyl-(Z)-α-acetamidocinnamate (eac), catalyzed by the rhodium complex of S,S-chiraphos (**C**).[4] A surprising conclusion (based on isolation and characterization of the major $[Rh(chiraphos)(eac)]^+$ diastereomer) was that the enantioselection in this system has its origin, not in the preferred mode of binding of the substrate to the catalyst but, rather, in the much higher reactivity toward H_2 of the minor (thermodynamically unfavorable) adduct. Thus, the predominant product enantiomer, N-acetyl-(R)-phenylalanine ethyl ester, is derived from the minor, rather than the major, diastereomer of the $[Rh(chiraphos)(eac)]^+$ precursor. In accord with this, and anticipating the result of the present study, Figure 2 depicts the major enantiomer of the product of the $[Rh(R,R\text{-dipamp})(mac)]^+$-catalyzed hydrogenation of mac, i.e., N-acetyl-(S)-phenylalanine methyl ester, as derived from the minor diastereomer of **2**.

A limitation of the study cited above was the fact that the ratio of the major to minor diastereomers of $Rh(chiraphos)(eac)]^+$ was

(1) For leading references, see: (a) Halpern, J. *Science (Washington, DC)* **1982**, *217*, 401. (b) Kagan, H. B. In *Comprehensive Organometallic Chemistry*; Wilkinson, G., Stone, F. G. A., Eds.; Pergamon: Oxford, 1982; Vol. 8, pp 463–498. (c) Bosnich, B.; Fryzuk, M. D. *Top. Stereochem.* **1981**, *12*, 119. (d) Knowles, W. S.; Chrisopfel, W. S.; Koenig, K. E.; Hobbs, C. F. *Adv. Chem. Ser.* **1982**, *196*, 325.

(2) (a) Halpern, J.; Riley, D. P.; Chan, A. S. C.; Pluth, J. J. *J. Am. Chem. Soc.* **1977**, *99*, 8055. (b) Chan, A. S. C.; Pluth, J. J.; Halpern, J. *Inorg. Chim. Acta* **1979**, *37*, L477. (c) Chan, A. S. C.; Halpern, J. *J. Am. Chem. Soc.* **1980**, *102*, 838.

(3) Halpern, J. In *Asymmetric Synthesis*; Morrison, J. D., Ed.; Academic Press: New York, 1985; Vol. 5, p 41, and references therein. This article presents a preliminary account of some of the conclusions of the present paper.

(4) (a) Chan, A. S. C.; Pluth, J. J.; Halpern, J. *J. Am. Chem. Soc.* **1980**, *102*, 5952. (b) Chua, P. S.; Roberts, N. K.; Bosnich, B.; Okrasinski, S. J.; Halpern, J. *J. Chem. Soc., Chem. Commun.* **1981**, 1278.

0002-7863/87/1509-1746$01.50/0

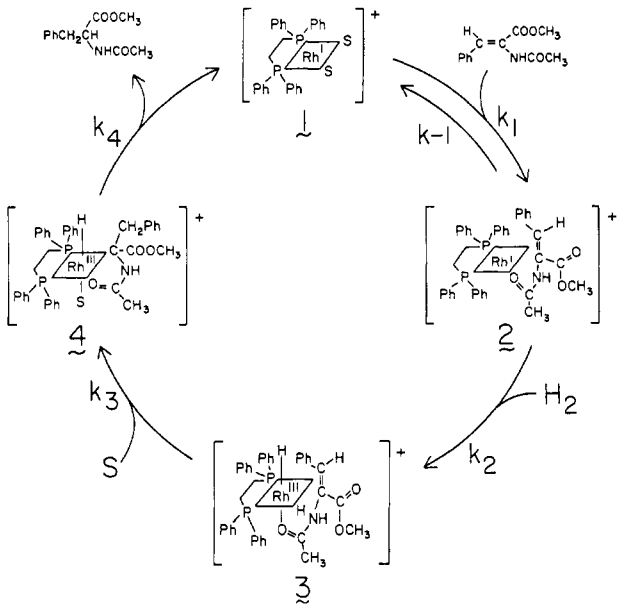

Figure 1. Catalytic cycle for the nonchiral catalyst, [Rh(diphos)$^+$].

so large (>20:1) that the minor diastereomer could not be observed. This severely constrained the information that could be deduced concerning the quantitative comparison of the two diastereomeric manifolds and of the factors that influence enantioselectivity. Accordingly, we now have examined the related hydrogenation of mac, catalyzed by the rhodium complex containing the chiral ligand, *R,R*-dipamp (**D**). In this system both the major and minor diastereomers of [Rh(dipamp)(mac)]$^+$ can be observed and both diastereomeric pathways, leading to the two enantiomeric products, monitored. The results of this study are reported in this paper. Specifically, we have attempted to address the following themes: (1) the origin of the enantioselection, (2) the origin and significance of the remarkable effects of the H_2 pressure on enantioselectivity that have been reported for several related catalytic systems,[5] and (3) the mechanism of interconversion of the diastereomeric adducts, $\mathbf{2}^{maj}$ and $\mathbf{2}^{min}$, and of crossover between the two diastereomeric manifolds.

To address these themes it was necessary to examine both the individual steps of the catalytic cycle encompassed by Figure 2 as well as the kinetics and enantioselection of the overall catalytic reaction. We report our experimental results in the following sequence: (1) kinetic and equilibrium measurements of the formation (and dissociation) of $\mathbf{2}^{maj}$ and $\mathbf{2}^{min}$, (2) measurements of the kinetics of the reaction of $\mathbf{2}^{maj}$ with H_2, and (3) measurements of the kinetics and enantioselectivity of the overall catalytic reaction.

Experimental Section

Reagents. H_2 (prepurified grade obtained from Linde Corp.), D_2 (Linde Corp.), and N_2 gases were freed of oxygen and water impurities by passage through columns of BASF R3-11 and Linde 13X molecular sieves. Ultrahigh purity grade hydrogen (Linde Corp.) was used without further purification.

Methanol (used as solvent in all the experiments) was purified by distillation from magnesium methoxide onto chromous chloride followed by vacuum transfer to a flask which was stored in an inert atmosphere glovebox. Diethyl ether and benzene were purified by distillation from sodium benzophenone ketyl under an inert atmosphere.

R,R-dipamp was generously supplied by Monsanto Co. Other phosphines were purified by passage through a silica gel column under an inert atmosphere, followed by recrystallization from acetone/petroleum ether. Norbornadiene was purified by distillation from activated alumina. 1-Hexene was purified by distillation from activated alumina under an inert atmosphere.

Syntheses. The compound, [Rh(*R,R*-dipamp)(nbd)][BF_4], was prepared according to Schrock and Osborn.[6] [Rh(*R,R*-dipamp)(mac)][BF_4] (as a mixture of $\mathbf{2}^{maj}$ and $\mathbf{2}^{min}$) was prepared according to Chan, Pluth, and Halpern.[4a] Methyl-(*Z*)-α-acetamidocinnamate was prepared according to Knowles et al.[7]

Preparation of [Rh(*R,R*-dipamp)][BF_4]. A slurry of [Rh(*R,R*-dipamp)(nbd)][BF_4] (0.25 g) in methanol (7.0 mL) was stirred under an H_2 atmosphere at room temperature until gas uptake ceased (ca. 15 min). The solution was cooled to −80 °C, evacuated, and diluted with diethyl ether (60 mL). After warming to room temperature, a golden-yellow precipitate deposited and was collected by filtration in an inert atmosphere. The precipitate (yield, 0.20 g) was washed with diethyl ether, dried in vacuo, and stored in an inert atmosphere.

Equilibrium Measurements. Measurement of Diastereomer Equilibrium Constant (K^{dias}). A 0.02 M solution of [Rh(*R,R*-dipamp)(mac)][BF_4] was sealed in a 10-mm NMR tube and placed in a thermostatted NMR probe for 15 min before pulsing was begun. ^{31}P NMR spectra were collected at constant temperature by using a 60° pulse, a 5-s delay period, and broad-band proton decoupling. The isomer ratio was determined from each spectrum by integration of the appropriate peaks; no corrections for NOE effects were made. The use of longer delay times yielded identical isomer ratios, indicating the absence of intensity anomalies due to relaxation differences between the two isomers.

Measurement of the Total Binding Constant (K_1^{tot}). An aliquot (3 mL) of a solution of [Rh(dipamp)][BF_4] (4.0×10^{-4} M in methanol) was loaded into a septum-capped silica spectrophotometric cell in an inert atmosphere glovebox and transferred into the thermostatted cell compartment of a UV–vis spectrophotometer. Carefully measured aliquots of a mac solution (2.81×10^{-2} M in methanol) were syringed into the sample cell, the cell was agitated briefly, and the UV–visible spectrum was recorded. Incremental additions of mac solution were continued until the endpoint was clearly passed. Isosbestic points for the spectral titration were observed at 362, 435, and 464 nm. The overall equilibrium constant, K^{tot}, was calculated from the absorbance changes at 400 nm.

Measurement of the Enantiomeric Excess. Samples for analysis of enantiomeric excess were drawn directly from the reaction solution and injected into a 1/8 in. × 6 ft. Supelco SP-301 GC column (5% on Supelcoport 60/80) operated isothermally at 125 °C and equipped with a flame-ionization detector. Essentially base line separation of *N*-acetylphenylalanine methyl ester enantiomers was obtained. Quantitation of the percent enantiomeric excess (expressed as $100 \times (S - R)/(S + R)$), was obtained by cutting and weighing the GC recordings.

Kinetic Measurements. Kinetics of the Low-Temperature Hydrogenation of [Rh(dipamp)(mac)][BF_4]. A 10-mm NMR tube was loaded with a 0.015 M solution of [Rh(dipamp)(mac)][BF_4] in methanol-d_4 and fitted with a rubber septum in the drybox. The sample tube was cooled to the desired temperature and then purged with a rapid flow of H_2 for a timed period. The gas was vented through a mercury bubbler which, in combination with the use of either pure H_2 or a 50:50 N_2:H_2 mixture, made possible measurements over a H_2 partial pressure range of 0.6–2.0 atm. At the end of the timed interval, the reaction was quenched rapidly by cooling to −80 °C and by changing the gas purge to N_2. After 10 min of N_2 purge at −80 °C the NMR tube was transferred to an NMR probe which was thermostatted at −80 °C. The ^{31}P NMR spectrum was recorded at −80 °C over a 1-h period. The hydrogenation reaction was then reinitiated by removing the sample tube from the NMR probe, placing it in a −80 °C thermostatted bath, purging with a rapid flow of H_2 for five minutes, and then placing the tube in a bath thermostatted at the reaction temperature for another timed interval. This procedure was repeated so that the reaction was monitored for a minimum of five time intervals covering approximately 2 half-lives. The disappearance of the major diastereomer of [Rh(dipamp)(mac)][BF_4] conformed to good first-order rate plots from the slopes of which pseudo-first-order rate constants (reproducible to within ±10%) were evaluated.

Determination of mac Association Rates ($k_1^{maj} + k_1^{min}$). The reservoirs of a thermostatted stopped-flow apparatus were adapted to utilize gas-tight syringes. These gas-tight syringes were loaded in an inert atmosphere glovebox with methanol solutions of [Rh(dipamp)][BF_4] and of mac. The syringes were sealed with Mininert valves and positioned in the stopped-flow apparatus (mixing time less than 1 ms) which was flushed with N_2. The reaction was monitored spectrophotometrically at 390 nm. Three kinetic traces were obtained for each set of reaction conditions with a typical reproducibility of the pseudo-first-order rate constants of ±1% of the mean value.

Measure of k_{-1}^{maj}. Methanol solutions of [Rh(dipamp)(mac)][BF_4] and of toluene or *p*-xylene were loaded into gas-tight syringes and fitted with Mininert valves in an inert atmosphere glovebox. These syringes were mounted in a thermostatted stopped-flow apparatus which was

(5) (a) Ojima, I.; Kogure, N.; Yoda, N. *J. Org. Chem.* **1980**, *45*, 4728. (b) Sinou, D. *Tetrahedron Lett.* **1981**, *22*, 2987.

(6) Schrock, R. R.; Osborn, J. A. *J. Am. Chem. Soc.* **1971**, *93*, 2397.

(7) Vineyard, B. D.; Knowles, W. S.; Sabacky, M. J.; Bachman, G. L.; Weinkauff, D. J. *J. Am. Chem. Soc.* **1977**, *99*, 5946.

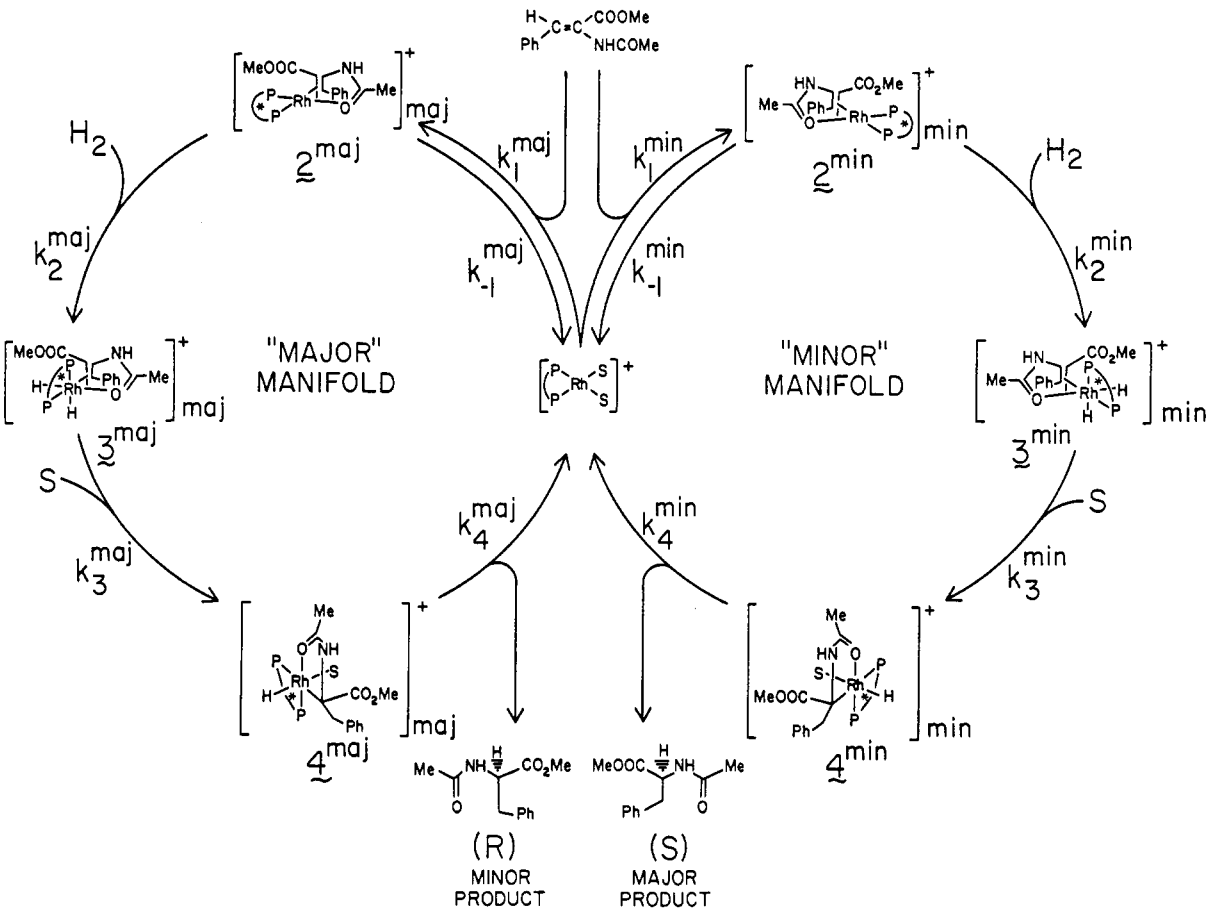

Figure 2. Mechanistic scheme for the $[Rh(dipamp)]^+$-catalyzed hydrogenation of mac.

back-flushed with N_2. The reaction was monitored by measuring the decrease in absorbance at 435 nm. Three kinetic traces were obtained for each set of conditions with typical reproducibility of the rate constants of ±1% of the mean value.

Constant Pressure Gas Uptake Measurements of the Catalytic Hydrogenation Rates. The H_2 gas uptake was measured with an apparatus comprising a magnetically stirred reactor, a pressure reference bulb, an oil manometer configured to indicate the reactor pressure relative to the reference bulb pressure, a calibrated gas piston, and a mercury manometer. All joints and valves were sealed with "O" rings. The entire apparatus was submerged in a constant temperature water bath. Reaction solutions were loaded into the reactor vessel in an inert atmosphere glovebox. The vessel was sealed by a high-vacuum valve and then connected to the gas uptake apparatus. Two freeze-pump-thaw cycles were performed, and the reactor was then thermally equilibrated for 5 min. When thermal equilibrium was reached, the apparatus was filled with a measured pressure of H_2, and agitation of the reaction solution was started. After 30 s of equilibration, the reference bulb was isolated from the reaction vessel by closing the interconnecting valve. Gas uptake, as indicated by displacement of the oil manometer levels, was offset by lowering the reaction vessel volume through compression of the calibrated piston. The piston volume displacement required to maintain constant pressure was measured as a function of time. The plots of gas uptake vs. time obtained in this manner were linear over 95% conversion of mac to the phenylalanine product enantiomers, and the slopes of these plots were reproducible to within ±5% of the mean value. The standard reaction rate was calculated from the following equation

$$\text{rate (M s}^{-1}) = -\text{d[mac]}/\text{dt} = \frac{-\text{d(vol H}_2)/\text{dt} \times P_{H_2}(\text{atm})}{\text{vol solution} \times R \times T(\text{K})} \quad (1)$$

Calculations of rate constants utilized the H_2 solubilities in methanol determined by Chan.[8]

Measurement of High-Pressure Hydrogenation Rates. A Fisher–Porter pressure bottle fitted with a pressure gauge and a sampling septum was charged with catalyst, substrate, and methanol in an inert atmosphere glovebox. The bottle was then connected to a vacuum line and a regulated hydrogen source via a T-connector. The solution was cooled to −80 °C, and the bottle was evacuated. The bottle was then placed in a temperature-controlled bath for a 20-min equilibration period. The reaction was initiated by the introduction of H_2 gas. At timed intervals samples were removed by means of a gas-tight syringe and quenched by exposure to air. The reaction was followed by measuring the conversion of mac to *N*-acetylphenylalanine methyl ester by NMR. Plots of *N*-acetylphenylalanine methyl ester vs. time were linear over 95% conversion, and the rate constants determined from the slopes of such plots were reproducible to within ±10% of the mean value.

(8) Chan, A. S. C. Ph.D. Dissertation, The University of Chicago, 1979.

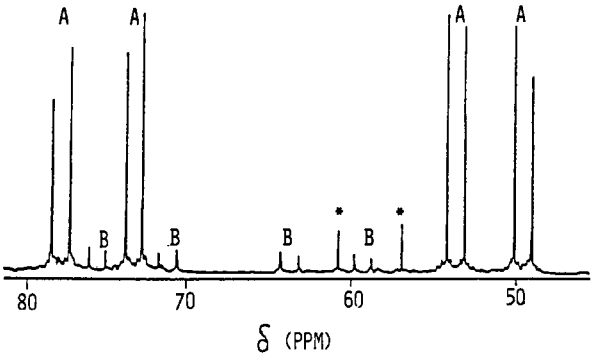

Figure 3. $^{31}P\{^1H\}$ NMR spectra of $[Rh(dipamp)(mac)]^+$ (**2**) at 29.6 °C: A, major diastereomer ($\mathbf{2}^{maj}$) δ_{P_1} = 51.3 ppm, $J_{P_1\text{-}Rh}$ = 150 Hz, $J_{P_1\text{-}P_2}$ = 39.5 Hz; δ_{P_2} = 74.7 ppm, $J_{P_2\text{-}Rh}$ = 162 Hz. B, minor diastereomer ($\mathbf{2}^{min}$) δ_{P_1} = 60.5 ppm, $J_{P_1\text{-}Rh}$ = 167 Hz, $J_{P_1\text{-}P_2}$ = 36.5 Hz; δ_{P_2} = 72.7 ppm, $J_{P_2\text{-}Rh}$ = 160.5 Hz. * = $[Rh(dipamp)_2^+]$ impurity (P_1 is trans to O=C; P_2 is trans to C=C).

Results

Determination of the Diastereomer Equilibrium Constant (K^{dias}). Dissolution of authentic [Rh(dipamp)(mac)][BF_4], or addition of 1 or more equiv of mac to a yellow solution of $[Rh(dipamp)]^+$, in methanol results in a deep red solution exhibiting the ^{31}P NMR spectrum shown in Figure 3. Two species having ABX spectral patterns with relative intensity patterns of ca. 10:1 are observed.[9]

Table I. Values of the Equilibrium Constant, K^{dias}

temp, °C	$K^{dias} = \frac{[Rh(dipamp)(mac)]^+_{maj}}{[Rh(dipamp)(mac)]^+_{min}}$
8.8	13.1
15.2	12.5
21.8	11.5
29.6	10.5
30.6	10.1
37.6	8.9
47.6	8.4

These species, whose ^{31}P NMR parameters are similar to those of the well-characterized complex $[Rh(diphos)(mac)]^+$,[2b] are identified as the diastereomeric adducts, $\mathbf{2}^{maj}$ and $\mathbf{2}^{min}$, with concentrations that are related through a temperature-dependent equilibrium (eq 2).

$$K^{dias} = [\mathbf{2}^{maj}]/[\mathbf{2}^{min}] = K_1{}^{maj}/K_1{}^{min} \quad (2)$$

where

$$K_1{}^{maj} = [\mathbf{2}^{maj}]/[\mathbf{1}][mac] = k_1{}^{maj}/k_{-1}{}^{maj} \quad (3)$$

and

$$K_1{}^{min} = [\mathbf{2}^{min}]/[\mathbf{1}][mac] = k_1{}^{min}/k_{-1}{}^{min} \quad (4)$$

Integration of the ^{31}P NMR peaks corresponding to $\mathbf{2}^{maj}$ and $\mathbf{2}^{min}$ allows the direct calculation of K^{dias} according to eq 2. The values of K^{dias}, measured over the temperature range 8.8–47.6 °C, are listed in Table I and yield the thermodynamic parameters, $\Delta H° = 2.2 \pm 0.1$ kcal/mol and $\Delta S° = 2.7 \pm 0.2$ cal/(mol K). In addition to the variation of relative peak intensities of $\mathbf{2}^{maj}$ and $\mathbf{2}^{min}$ as a function of temperature, the line widths of the peaks corresponding to $\mathbf{2}^{min}$, but not $\mathbf{2}^{maj}$, were observed to broaden slightly at higher temperatures. While this feature was not studied in detail, this observation does seem to suggest a faster eneamide exchange, a dissociative process, for $\mathbf{2}^{min}$ than for $\mathbf{2}^{maj}$.

Determination of the Total Binding Constant ($K_1{}^{tot}$). The formation of the red diastereomers, $\mathbf{2}^{maj}$ and $\mathbf{2}^{min}$, from the yellow complex, $[Rh(dipamp)(S)_2]^+$ (**1**), attains an equilibrium that is conveniently monitored by UV–vis spectroscopy. The spectra obtained on titration of a methanol solution of **1** with a methanol solution of mac exhibit isosbestic points at 362, 435, and 464 nm with a maximum change in molar absorptivity at 400 nm, [ϵ_{400}(**1**) = 1.14×10^3 M^{-1} cm^{-1}, ϵ_{400}(equilibrium mixture of $\mathbf{2}^{maj}$ and $\mathbf{2}^{min}$) = 2.37×10^3 M^{-1} cm^{-1} at 25 °C.] The equilibria investigated by this spectral titration are defined by eq 3–7. From the spectral

$$mac + \mathbf{1} \overset{K_1{}^{maj}}{\rightleftharpoons} \mathbf{2}^{maj} \quad (5)$$

$$mac + \mathbf{1} \overset{K_1{}^{min}}{\rightleftharpoons} \mathbf{2}^{min} \quad (6)$$

$$K_1{}^{tot} = K_1{}^{min} + K_1{}^{maj} \quad (7)$$

data, the equilibrium constant, $K_1{}^{tot}$, at 25 °C was determined to be $(3.7 \pm 0.9) \times 10^4$ M^{-1}, a value similar to those previously determined for the corresponding formation constants of $[Rh(diphos)(mac)]^+$ ($K = 2.1 \times 10^4$ M^{-1}) and $[Rh(chiraphos)(mac)]^+$ ($K = 3.2 \times 10^4$ M^{-1}).[15]

Measurement of mac Binding Rates. The equilibria defined by eq 5 and 6 are rapidly established, necessitating the use of stopped-flow methods to measure the rates of approach to equilibrium. Rapid mixing of methanol solutions of **1** and mac in a stopped-flow spectrophotometer resulted in a rapid increase in the absorbance at 400 nm, the rate of which was measurable when the mac concentration was less than 1×10^{-2} M. Measurements of the kinetics of equilibration were made under pseudo-first-order conditions (excess mac). It was found that (1) the individual kinetic traces were strictly first-order over 4 half-lives and yielded the correct absorbance changes based on spectral titration data and (2) the pseudo-first-order rate constants (k_{obsd}) were proportional to the mac concentrations (Table II), in accord with the rate law

$$-d\ln[\mathbf{1}]/dt = k_{obsd} = k^{assoc}[mac] \quad (8)$$

Since the equilibrium constants for formation of the $[Rh(dipamp)(mac)]^+$ adducts are very large ($>10^3$ M^{-1}), only the forward (i.e., associative) rates are accessible to measurement by this method. Furthermore, the stopped-flow measurements yielded only the combined rate constant (k^{assoc}) for formation of an equilibrium mixture of the diastereomeric adducts, $\mathbf{2}^{maj}$ and $\mathbf{2}^{min}$, i.e.,

$$k^{assoc} = k_1{}^{maj} + k_1{}^{min} \quad (9)$$

The values of k^{assoc}, listed in Table II, are similar to those determined previously for binding of mac to $[Rh(diphos)(S)_2]^+$ ($k_1 = 1.4 \times 10^4$ M^{-1} s^{-1} at 25 °C).[8] The temperature dependence (25–41.3 °C) of k^{assoc} yields the apparent activation parameters: $\Delta H^‡ = 6.9 \pm 0.9$ kcal/mol, $\Delta S^‡ = -18 \pm 2$ cal/(mol K).

Measurement of the mac Dissociation Rate. We have found that the rate of dissociation of mac from a mixture of $\mathbf{2}^{maj}$ and $\mathbf{2}^{min}$ can be measured by trapping the intermediate $[Rh(dipamp)(S)_2]^+$ (**1**) with another strongly binding ligand, such as toluene.[2a,11] When a solution of $\mathbf{2}^{maj}$ and $\mathbf{2}^{min}$ was mixed with

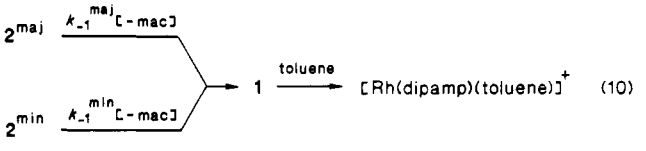

a methanol solution of toluene in a stopped-flow spectrophotometer, the deep red color of the eneamide complex was rapidly bleached to give a pale yellow solution (half-life ca. 4 s at 25 °C). The visible spectrum of the resulting solution was identical with a solution of **5** generated by addition of toluene to a methanol solution of **1**. The changes in absorbance as a function of time are accommodated by a simple first-order rate law (eq 11).

$$d[Rh(dipamp)(arene)^+]/dt = k_{11}[Rh(dipamp)(mac)^+] \quad (11)$$

Values of k_{11} for different arene concentrations, arene types (toluene and *p*-xylene), and temperatures are listed in Table III.

Table II. Kinetic Data for the Reaction of $[Rh(dipamp)(S_2)]^+$ with mac

$[Rh(dipamp(S)_2]^+$, M	[mac], M	temp, °C	k_{obsd}, s^{-1}	$k_{obsd}/$[mac], M^{-1} s^{-1}
2.31×10^{-1}	3.9×10^{-3}	25.0	63.4	1.63×10^4
	8.6×10^{-3}	25.0	147	1.71×10^4
	1.9×10^{-2}	25.0	297	1.57×10^4
	3.9×10^{-3}	30.0	82	2.10×10^4
	3.9×10^{-3}	37.1	96	2.46×10^4
	3.9×10^{-3}	41.2	118	3.03×10^4

Table III. Kinetic Data for the Reaction of $[Rh(dipamp)(mac)]^+$ with Arenes

$[Rh(dipamp(mac)]_0^+$, M	arene	[arene], M	temp, °C	k_{obsd}, s^{-1}
4.1×10^{-4}	toluene	0.38	25.0	0.150
	toluene	0.94	25.0	0.146
	toluene	1.41	25.0	0.145
	p-xylene	0.81	25.0	0.143
	toluene	0.94	30.2	0.202
	toluene	0.94	35.0	0.280
	p-xylene	0.81	35.6	0.289
	toluene	1.41	38.0	0.400
	toluene	0.94	41.3	0.470
	toluene	0.94	45.3	0.605
	toluene	1.41	45.8	0.720

(9) Similar spectra have previously been observed for the diastereomeric adducts, [Rh(*R*,*R*-dipamp)(methyl-(*Z*)-α-benzamidocinnamate)]+.[10]

(10) Brown, J. M.; Chaloner, P. A. *Tetrahedron Lett.* **1978**, 1877.
(11) Brown, J. M.; Chaloner, P. A. *J. Chem. Soc., Chem. Commun.* **1980**, 344.

Table IV. Kinetic Data for the Low-Temperature Reaction of $[Rh(dipamp)(mac)]^+_{maj}$

$[Rh]_{tot}$, M	P_{H_2}, atm	temp, °C	$10^4 k_{obsd}$, s^{-1}	$10^4 k_{14}^{calcd}$,[a] s^{-1}
1.5×10^{-2}	0.6	−35.6	1.1	1.4
	0.6	−35.6	1.3	1.4
	1.2	−35.6	1.3	1.4
	1.8	−35.6	1.4	1.4
	1.2	−25.2	6.2	5.3
	1.2	−30.6	3.3	2.6
	1.2	−39.6	0.75	0.73

[a] From eq 16 and data in Table VI.

k_{11} is seen to be independent of the arene type and concentration. This supports a dissociative replacement mechanism (eq 10) in which the arene serves as an efficient trap for **1**.

The formation of the arene adduct **5** by dissociation of mac from two chemically distinct mac adducts, $\mathbf{2}^{maj}$ and $\mathbf{2}^{min}$, should give rise to a biexponential absorbance curve for the conversion of $\mathbf{2}^{maj}$ and $\mathbf{2}^{min}$ into **5**. The contribution to this curve from reaction of $\mathbf{2}^{maj}$, in accordance with the equilibrium distribution of $\mathbf{2}^{maj}$ and $\mathbf{2}^{min}$, is expected to be 10.7 times greater than the contribution of $\mathbf{2}^{min}$. Furthermore, it is likely that k_{-1}^{min} is larger (significant ^{31}P NMR line broadening) than k_{-1}^{maj} (no ^{31}P NMR line broadening). Thus, we assign the observed rate constant for the simple exponential growth of **5** (i.e., k_{11}) to k_{-1}^{maj}, the rate constant for mac dissociation from $\mathbf{2}^{maj}$. The dissociation of mac from the minor diastereomer, $\mathbf{2}^{min}$, apparently is obscured because of its relatively small contribution to the total absorbance change and because of the faster time scale for that transformation. Accordingly, k_{-1}^{maj} is deduced to be 0.15 ± 0.1 s^{-1} at 25 °C (Table III). The temperature dependence of k_{-1}^{maj} yields the activation parameters, $(\Delta H^{\ddagger}_{-1})^{maj} = 13.3 \pm 0.5$ kcal/mol and $(\Delta S^{\ddagger}_{-1})^{maj} = 18 \pm 1$ cal/(mol K).

Stoichiometric Reaction of H_2 with $[Rh(dipamp)(mac)]^+$ at Low Temperatures. The temperature dependence of the equilibrium between $\mathbf{2}^{maj}$ and $\mathbf{2}^{min}$ is such that only $\mathbf{2}^{maj}$ is observed (by NMR) at temperatures below −10 °C. Exposure of such solutions of $\mathbf{2}^{maj}$ to H_2 at temperatures between −25 and −40 °C resulted, initially, in a decrease in a concentration of $\mathbf{2}^{maj}$ and the appearance of a new set of ^{31}P NMR signals (Figure 4; δ P_1 = 73.7 ppm, J_{P_1-Rh} = 137 Hz, δ P_2 = 60.0 ppm, J_{P_2-Rh} = 98 Hz, $J_{P_1-P_2}$ = 11 Hz) similar to that reported for the alkyl hydride derived from the benzamido analogue of $\mathbf{2}^{min}$ (i.e., $\mathbf{4}^{min}$).[12] Further exposure of H_2 resulted in the disappearance of $\mathbf{2}^{maj}$ and, ultimately, of $\mathbf{4}^{min}$, with accumulation of $[Rh(dipamp)(S)_2]^+$ (**1**). The rate of disappearance of $\mathbf{2}^{maj}$ at constant H_2 pressures, monitored by ^{31}P NMR spectroscopy, conformed to pseudo-first-order kinetics, yielding the rate constants listed in Table IV. These are seen to be essentially independent of the H_2 concentration.

Kinetics of Catalytic Hydrogenation. The catalytic hydrogenation of mac, using $[Rh(dipamp)(nbd)]^+$ as the catalyst precursor, was initiated by rapid hydrogenation of nbd to produce a deep red solution of the mac adducts, $\mathbf{2}^{maj}$ and $\mathbf{2}^{min}$. The rate of catalytic hydrogenation, monitored by measuring the uptake of H_2 at constant pressure, was found to be pseudo-zero-order in the concentration of mac until the latter was consumed (Figure 5). The pseudo-zero-order rate constants are listed in Table V and are seen to be first order in the concentration of the Rh catalyst and independent of the concentration of mac, in agreement with the behavior reported previously for the hydrogenation of mac catalyzed by the achiral catalyst, $[Rh(diphos)(mac)]^+$.[2c] Table V also lists the enantiomeric excess (of *S* product over *R*) in each experiment. The H_2 pressure and temperature dependencies of the rate and enantioselectivity, reported in Table V and in Figures 6–8, are complex and are discussed below.

The rate constants and corresponding activation parameters for the various steps of the catalytic scheme are summarized in Table VI.

(12) Brown, J. M.; Chaloner, P. A.; Morris, G. A. *J. Chem. Soc., Chem. Commun.* **1983**, 664.

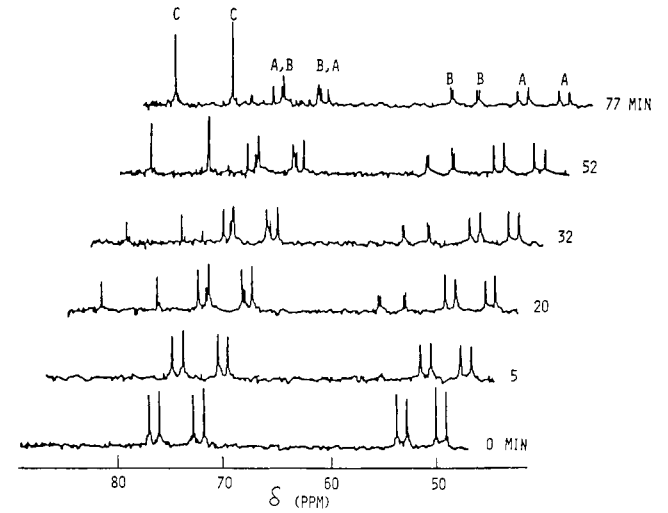

Figure 4. $^{31}P\{^1H\}$ NMR spectra for the reaction of $[Rh(dipamp)(mac)]^+_{maj}$ with H_2 at −35 °C: A, $[Rh(dipamp)(mac)]^+_{maj}$; B, $[Rh(dipamp)(H)(HMAC)]^+_{min}$; C, $[Rh(dipamp)(S)_2]^+$.

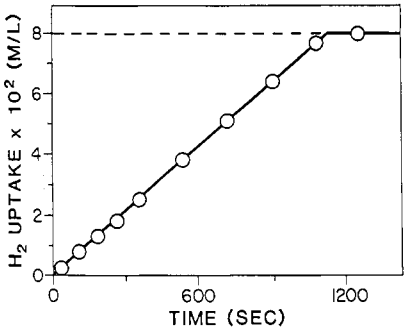

Figure 5. Plot of H_2 uptake vs. time for the $[Rh(dipamp)]^+$-catalyzed hydrogenation of mac at 25.0 °C: $[Rh]_{tot} = 5.1 \times 10^{-4}$ M; initial [mac] = 0.080 M; H_2 pressure = 1.1 atm.

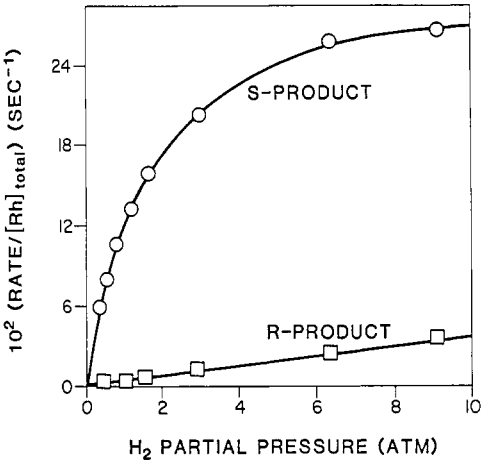

Figure 6. Dependence of the rate on the H_2 pressure for the $[Rh(dipamp)]^+$-catalyzed hydrogenation of mac at 25 °C.

Discussion

Mechanism of Interconversion of the Diastereomeric Adducts ($\mathbf{2}^{maj} \rightleftharpoons \mathbf{2}^{min}$). The mechanism of interconversion of the diastereomeric $[Rh(dipamp)(mac)]^+$ adducts ($\mathbf{2}^{maj} \rightleftharpoons \mathbf{2}^{min}$) may be deduced from our determination of the kinetics and products of the stoichiometric reaction of H_2 with $\mathbf{2}^{maj}$ at low temperatures. Brown and Chaloner[11] have reported that the reaction of H_2 with nonequilibrium mixtures of the benzamido analogues of $\mathbf{2}^{maj}$ and $\mathbf{2}^{min}$ at −55 °C leads to the rapid disappearance of $\mathbf{2}^{min}$ and formation of the corresponding alkyl hydride, $\mathbf{4}^{min}$, while $\mathbf{2}^{maj}$ does not react. Two features of our observations on the reaction of H_2 with $\mathbf{2}^{maj}$ at temperatures from −25 to −40 °C (Figure 4 and Table IV) convincingly demonstrate that the formation of $\mathbf{4}^{min}$

Table V. Kinetic Data and Enantioselectivities for the $[Rh(dipamp)(S)_2]^+$-Catalyzed Hydrogenation of mac

$[Rh]^{tot}$, M	$[mac]_0$, M	P_{H_2}, atm	temp, °C	rate, M s^{-1}	rate/$[Rh]_{tot}$, s^{-1}	ee, %[a]
1.1×10^{-4}	0.20	0.33	25.0	0.70×10^{-5}	6.4×10^{-2}	96.2
2.5×10^{-4}		0.35		1.55×10^{-5}	6.2×10^{-2}	96.0
5.1×10^{-4}	0.40	0.32		3.20×10^{-5}	6.3×10^{-2}	95.7
	0.20	0.51		4.01×10^{-5}	8.0×10^{-2}	95.0
		0.83		5.63×10^{-5}	1.1×10^{-1}	94.2
		1.10		7.15×10^{-5}	1.4×10^{-1}	92.0
4.5×10^{-4}	0.40	1.60		7.47×10^{-5}	1.7×10^{-1}	92.1
		2.95		9.52×10^{-5}	2.1×10^{-1}	91.7
		6.35		1.29×10^{-4}	2.9×10^{-1}	80.6
		9.07		1.29×10^{-4}	2.9×10^{-1}	73.8
7.5×10^{-4}	0.10	0.16	0.0	3.83×10^{-6}	5.1×10^{-3}	97.2
		0.42		6.69×10^{-6}	8.9×10^{-3}	95.2
		0.72		9.90×10^{-6}	1.3×10^{-2}	94.1
		0.83		1.06×10^{-5}	1.4×10^{-2}	92.0
		1.26		1.10×10^{-5}	1.5×10^{-2}	90.0
		1.77		1.35×10^{-5}	1.4×10^{-2}	88.6
7.5×10^{-4}	0.10	0.27	14.8	1.56×10^{-5}	2.1×10^{-2}	95.3
		0.71		2.98×10^{-5}	3.9×10^{-2}	94.9
		1.03		3.74×10^{-5}	5.0×10^{-2}	92.9
		1.64		4.51×10^{-5}	6.0×10^{-2}	91.4
2.2×10^{-4}	0.40	1.45	37.0	7.31×10^{-5}	3.3×10^{-1}	93.8
		1.79		7.73×10^{-5}	3.5×10^{-1}	92.6
		2.81		1.00×10^{-4}	4.5×10^{-1}	89.9
		5.12		1.25×10^{-4}	5.6×10^{-1}	87.3
		8.57		1.52×10^{-4}	6.8×10^{-1}	82.3

[a] ee = $100(S-R)/(S+R)$.

Table VI. Rate Constants and Activation Parameters for the $[Rh(dipamp)]^+$-Catalyzed Hydrogenation of mac

temp, °C	k_1^{min}, M^{-1} s^{-1}	k_1^{maj}, M^{-1} s^{-1}	k_{-1}^{min}, s^{-1}	k_{-1}^{maj}, s^{-1}	k_2^{min}, M^{-1} s^{-1}	k_2^{maj}, M^{-1} s^{-1}
0.0	$(3.3 \pm 0.3) \times 10^3$	$(2.5 \pm 0.2) \times 10^3$	0.34 ± 0.02	$(1.6 \pm 0.2) \times 10^{-2}$	$(1.70 \pm 0.1) \times 10^2$	0.18 ± 0.02
14.7	$(6.5 \pm 0.5) \times 10^3$	$(4.4 \pm 0.3) \times 10^3$	1.1 ± 0.1	$(6.1 \pm 0.4) \times 10^{-2}$	$(3.3 \pm 0.2) \times 10^2$	0.44 ± 0.03
25.0	$(1.06 \pm 0.06) \times 10^4$	$(5.3 \pm 0.4) \times 10^3$	3.2 ± 0.2	$(1.5 \pm 0.1) \times 10^{-1}$	$(6.3 \pm 0.5) \times 10^2$	1.1 ± 0.1
37.0	$(1.7 \pm 0.1) \times 10^4$	$(8.8 \pm 0.9) \times 10^3$	6.3 ± 0.4	$(3.5 \pm 0.2) \times 10^{-1}$	$(9.5 \pm 0.7) \times 10^2$	1.9 ± 0.2
$\Delta H^{\ddagger}$ (kcal/mol)	6.9 ± 0.2	4.9 ± 0.5	13.0 ± 0.7	13.3 ± 0.5	7.5 ± 0.5	10.7 ± 0.9
$\Delta S^{\ddagger}$ (cal/mol K)	-17.0 ± 0.4	-24.6 ± 1.9	-12.9 ± 0.9	-17.9 ± 0.9	-20.8 ± 1.3	-22.6 ± 2.8
interpolated value[a]	1.05×10^4	5.9×10^3	2.9	0.15	5.8×10^2	1.0

[a] Rate Constants at 25 °C calculated from activation parameters.

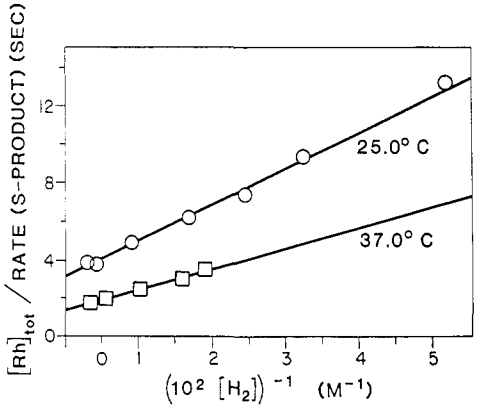

Figure 7. H_2 pressure-dependence of the rate of formatiom of *N*-acetyl-*S*-phenylalanine methyl ester plotted according to eq 25.

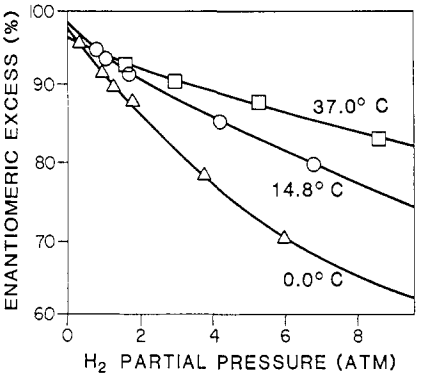

Figure 8. Effect of temperature and H_2 pressure on the enantioselectivity of the $[Rh(dipamp)]^+$-catalyzed hydrogenation of mac.

occurs not by direct reaction of $\mathbf{2}^{maj}$ with H_2 but, rather according to eq 12, by isomerization of $\mathbf{2}^{maj}$ to $\mathbf{2}^{min}$ followed by rapid trapping of the latter by H_2. These are (1) the product of the reaction is $\mathbf{4}^{min}$ rather than $\mathbf{4}^{maj}$ and (2) the rate of reaction is independent of the H_2 concentration.

$$\mathbf{2}^{maj} \xrightarrow{k_{12}} \mathbf{2}^{min} \xrightarrow{H_2} \mathbf{4}^{min} \qquad (12)$$

Furthermore, our independent determination of the rate constants k_1^{maj}, k_1^{min}, and k_{-1}^{maj} permits the elucidation of the mechanism of the isomerization of $\mathbf{2}^{maj}$ to $\mathbf{2}^{min}$. If this isomerization occurs by the dissociative intermolecular mechanism of the scheme in Figure 2 (eq 13) the apparent rate constant (k_{14}) is given by the steady-state expression of eq 14. Values of k_{14},

$$\mathbf{2}^{maj} \underset{k_1^{maj}}{\overset{k_{-1}^{maj}}{\rightleftharpoons}} \mathbf{1} + mac \xrightarrow{k_1^{min}} \mathbf{2}^{min} \qquad (13)$$

$$k_{14} = \frac{-d\ln[2^{maj}]}{dt} = \frac{k_{-1}^{maj} k_1^{min}}{k_1^{maj} + k_1^{min}} \qquad (14)$$

calculated by using this expression, and the values of k_{-1}^{maj}, k_1^{maj}, and k_1^{min}, deduced from the independently determined kinetic parameters in Table VI, are listed in Table IV and are seen to be in excellent agreement with the measured values. This demonstrates that the interconversion of $\mathbf{2}^{maj}$ and $\mathbf{2}^{min}$ occurs predominantly by the dissociative mechanism of Figure 2 (eq 13) and that the contribution of intramolecular pathways to this conversion, if any, is small. This contrasts with the conclusion of Brown, Chaloner, and Morris[12] that the interconversion of [Rh(dipamp)(methyl-(*Z*)-α-benzamidocinnamate)]$^+$ at 50 °C occurs predominantly through an *intramolecular* pathway. (An approximately 5:1 ratio of rates of intramolecular to intermolecular isomerization can be estimated from their rate data.) The reasons for this difference are not clear and may be related to differences in the enamide or the temperature.

Kinetics and Mechanism of Catalytic Hydrogenation. The mechanism of asymmetric hydrogenation, depicted in Figure 2, encompasses four component steps: (a) reversible binding of the substrate (mac) to the catalyst, (b) irreversible[3] oxidative addition of H_2 to the rhodium–substrate complex, (c) irreversible[3] insertion of the alkene into a metal–hydrogen bond, and (d) irreversible reductive elimination of the product amino acid ester. All of these steps occur along parallel, diastereomeric pathways (Figure 2). From previous measurements on both achiral and chiral catalysts it is known that the insertion of the C=C bond into the Rh–H bond is very rapid. (Even at temperatures as low as −95 °C, the addition of H_2 to [Rh(diphosphine)(mac)]$^+$ proceeds directly to the alkyl hydride complex without any observable accumulation of the dihydride intermediate.[2,4,13]) The reductive elimination step can occur slowly enough for observable accumulation of the alkyl hydride intermediate but only at temperatures below −25 °C (see previous section). Thus, only the substrate binding and the oxidative addition steps for the two diastereomeric pathways need be considered in describing the kinetics under ambient conditions.

Application of the steady-state treatment to the catalytic cycle of Figure 2 yields the rate law[13]

$$\text{rate} = -\text{d}[\text{H}_2]/\text{dt} = \left[\frac{k_2^{maj}k_1^{maj}}{k_{-1}^{maj} + k_2^{maj}[\text{H}_2]} + \frac{k_2^{min}k_1^{min}}{k_{-1}^{min} + k_2^{min}[\text{H}_2]}\right] \times \left[\frac{[\text{Rh}]_{tot}[\text{mac}][\text{H}_2]}{1 + \frac{k_1^{maj}[\text{mac}]}{k_{-1}^{maj} + k_2^{maj}[\text{H}_2]} + \frac{k_1^{min}[\text{mac}]}{k_{-1}^{min} + k_2^{min}[\text{H}_2]}}\right] \quad (15)$$

At sufficiently low H_2 pressures (i.e., when $k_1^{maj} >> k_2^{maj}[H_2]$ and $k_{-1}^{min} >> k_2^{min}[H_2]$) the oxidative addition of H_2 is much slower than dissociation of mac from the major and minor diastereomeric adducts ($\mathbf{2}^{maj}$ and $\mathbf{2}^{min}$), so that the kinetic behavior corresponds to diastereomeric preequilibrium binding steps followed by turnover-limiting diastereomeric oxidative addition steps. Since the binding equilibrium constants are large ($\sim 10^4$ M^{-1}), the preequilibrium steps are saturated (i.e., $[\mathbf{2}^{maj}] + [\mathbf{2}^{min}] \approx [\text{Rh}]_{tot}$), and the rates of the diastereomeric pathways are given by the equations

$$\text{total rate} = -\text{d}[\text{H}_2]/\text{dt} = \frac{(k_2^{maj}K_1^{maj}[\text{H}_2] + k_2^{min}K_1^{min}[\text{H}_2])[\text{Rh}]_{tot}}{K_1^{maj} + K_1^{min}} \quad (16)$$

$$\text{d}[R\text{-product}]/\text{dt} = k_2^{maj}K_1^{maj}[\text{H}_2][\text{Rh}]_{tot}/(K_1^{maj} + K_1^{min}) \quad (17)$$

$$\text{d}[S\text{-product}]/\text{dt} = k_2^{min}K_1^{min}[\text{H}_2][\text{Rh}]_{tot}/(K_1^{maj} + K_1^{min}) \quad (18)$$

(13) Landis, C. L. Ph.D. Dissertation, The University of Chicago, 1983.

Under these conditions, the enantioselectivity is given by the ratios of the product of the preequilibrium constant and the oxidative addition rate constants for the two pathways. Since the minor diastereomer gives rise to the major product, i.e., *N*-acetyl-*S*-phenylalanine methyl ester, the product ratios are given by

$$\frac{[S\text{-phenylalanine}]}{[R\text{-phenylalanine}]} = \frac{k_2^{min}K_1^{min}}{k_2^{maj}K_1^{maj}} \quad (19)$$

$$\text{enantiomeric excess (ee \%)} = (S - R)/(S + R) \quad (20)$$

In the limit of infinitely high H_2 pressure, the oxidative addition step becomes much faster than the binding steps ($k_2[H_2] >> k_{-1}$, k_1[mac]), and the reaction rate and enantioselectivity are determined by the mac association step. In this limit, the rate and enantioselectivity are independent of the H_2 concentration.[14]

$$\text{rate} = -\text{d}[\text{H}_2]/\text{dt} = k_1^{maj}[\text{Rh}]_{tot}[\text{mac}] + k_1^{min}[\text{Rh}]_{tot}[\text{mac}] \quad (21)$$

$$\frac{[S\text{-phenylalanine}]}{[R\text{-phenylalanine}]} = \frac{k_1^{min}}{k_1^{maj}} \quad (22)$$

The rate law and enantioselectivity at intermediate H_2 pressures are complex since they are functions of the rates of the six kinetically relevant steps. Fortunately, the cumbersome steady-state expression can be simplified to a useable (and verifiable!) form by making a few reasonable assumptions. Upon increasing the H_2 pressure, deviation of the rate and enantioselection from the low-pressure limit occurs when $k_2[H_2] \sim k_{-1}$. Because the rates of oxidative addition of H_2 (the enantio-determining step) for the two diastereomeric pathways are so different, the onset of competition of oxidative addition with olefin dissociation occurs at different pressures for the two diastereomeric pathways. Since $k_2^{min} >> k_2^{maj}$, the onset of such a competition occurs at a lower pressure for the minor diastereomeric pathway than for the major diastereomer ($k_2^{maj}[H_2] \ll k_{-1}^{maj}$ when $k_2^{min}[H_2] = k_{-1}^{min}$). Under these conditions, the major diastereomer will still be the predominant catalyst species, $[\mathbf{2}^{maj}]$ ($\propto K^{maj}$) >> $[\mathbf{2}^{min}]$ ($\propto k_1^{min}/k_{-1}^{min} + k_2^{min}[H_2]$). In this regime the rate for the major diastereomeric pathway still is given by the low H_2 pressure-limiting rate law (eq 23) whereas the rate of the minor diastereomer pathway is given by the steady-state expression of eq 24; the latter rearranges to eq 25.

$$\text{d}[R\text{-product}]/\text{dt} = k_2^{maj}[\text{Rh}]_{tot}[\text{H}_2] \quad (23)$$

$$\text{d}(S\text{-product})/\text{dt} = \frac{k_2^{min}k_1^{min}[\text{Rh}]_{tot}[\text{H}_2]}{K_1^{maj}(k_{-1}^{min} + k_2^{min}[\text{H}_2])} \quad (24)$$

$$\frac{[\text{Rh}]_{tot}}{\text{d}[S\text{-product}]/\text{dt}} = \frac{K_1^{maj}k_{-1}^{min}}{k_1^{min}k_2^{min}[\text{H}_2]} + \frac{K_1^{maj}}{k_1^{min}} \quad (25)$$

Thus, the rate corresponding to the major diastereomer pathway, which contributes only a small fraction of the total product, remains first-order in H_2 in the pressure regime where the rate of the minor diasteromer pathway is becoming independent of the H_2 pressure. Accordingly, as the H_2 pressure is increased, the total reaction rate is expected to level off and the enantioselectivity to decrease. This behavior is depicted in Figure 6. The linear plots $[\text{Rh}]_{tot}/(\text{d}[S\text{-product}]/\text{dt})$ vs. $1/[\text{H}_2]$ in Figure 7 are in accord with eq 25 and yield $K_1^{maj}/k_1^{min} = 3.4 \pm 0.3$ s and $k_{-1}^{min}/k_2^{min} = (5.0 \pm 0.3) \times 10^{-3}$ M at 25 °C. The observed dependence of the rate and enantioselectivity on the H_2 pressure

(14) The enantioselectivity actually becomes independent of the H_2 pressure at a somewhat lower H_2 pressure than that required for the rate to be independent of H_2 pressure. When the rate of oxidative addition becomes much faster than the rate of mac dissociation ($k_2[H_2] >> k_1$), the interconversion of $\mathbf{2}^{maj}$ and $\mathbf{2}^{min}$ is essentially frozen out, and the enantioselection is determined by the rates of formation of $\mathbf{2}^{maj}$ and $\mathbf{2}^{min}$ (eq 21). Since $k_{-1} << k_1$[mac] under normal conditions, the H_2 pressure required for a H_2 pressure-independent enantioselectivity ($k_2[H_2] >> k_{-1}$) is lower than that required for a H_2 pressure-independent rate ($k_2[H_2] >> k_1$[mac]).

supports the mechanism proposed in Figure 2 and provides the first convincing and quantitative explanation of the leveling effect of the enantiomeric excess with increasing H_2 pressure.

The parameters obtained from the kinetics of the catalytic hydrogenation reaction (k_2^{maj}, K_1^{maj}/k_1^{min}, $K_1^{maj}/K_1^{min}k_2^{min}$), together with the parameters obtained from stoichiometric reaction kinetics and equilibrium measurements (K^{dias}, k_{-1}^{min}, $k_1^{maj} + k_1^{min}$, K^{tot}), permit determination of the six independent rate constants from seven independent, nonredundant, equations (eq 26–32, values at 25 °C). The individual rate constants, calculated from

$$K_1^{tot} = (3.7 \pm 0.9) \times 10^4\ M^{-1} \quad (26)$$

$$K^{dias} = K_1^{maj}/K_1^{min} = 10.7 \pm 0.2 \quad (27)$$

$$k_{-1}^{min} = 0.15 \pm 0.007\ s^{-1} \quad (28)$$

$$k_1^{maj} + k_1^{min} = (1.59 \pm 0.08) \times 10^4\ M^{-1}\ s^{-1} \quad (29)$$

$$k_2^{maj} = (1.1 \pm 0.15)\ M^{-1}\ s^{-1} \quad (30)$$

$$\frac{K_1^{maj}}{k_1^{min}} = \frac{k_1^{maj}}{k_1^{min}\,k_{-1}^{maj}} = (3.4 \pm 0.4)\ s \quad (31)$$

$$\frac{k_{-1}^{min}}{k_2^{min}} = (5.0 \pm 0.3) \times 10^{-3}\ M \quad (32)$$

these equations (the least accurate parameter, K_1^{tot}, was not used in the calculation), are listed in Table VI, together with the corresponding activation parameters. The ratio of the H_2 oxidative addition rate constants, k_2^{min}/k_2^{maj}, is 580 at 25 °C, whereas K^{dias} = 10.7 (= $[\mathbf{2}^{maj}]/[\mathbf{2}^{min}]$). This dramatically demonstrates that the enantioselection is determined by the relative rates of reaction of the diastereomeric adducts with H_2 rather than by the relative rates or equilibrium constants for binding of the prochiral substrate to the chiral catalyst. The value of $K^{tot} = (3.7 \pm 0.9) \times 10^4\ M^{-1}$ obtained by spectral titration compares favorably with the value determined from the individual rate constants $k_1^{min}/k_{-1}^{min} + k_1^{maj}/k_{-1}^{maj} = (4 \pm 1) \times 10^4\ M^{-1}$ and provides further confirmation of the validity of the mechanistic interpretation.

The mechanism of Figure 2 can be tested further by comparing experimental measurements of enantioselectivity at high pressures with values calculated from our independently determined rate constants (Table VI) by using eq 22. It has been found that with increasing H_2 partial pressures the enantioselectivity of the [Rh(dipamp)(mac)]$^+$-catalyzed hydrogenation of mac decreases to a limiting value of approximately 25% at H_2 pressures $\gtrsim$200 atm at 25 °C.[15] From the rate constants in Table VI, $k_2^{maj}[H_2]$ at 200 atm H_2 is calculated to be 0.75 s^{-1}. This is sufficiently larger than k_{-1}^{maj} (0.15 s^{-1} at 25 °C) to represent approach to the high H_2 pressure limit. From the value of $k_1^{min}/k_1^{maj} = 1.8 \pm 0.2$, the enantiomeric excess of the *S*-product is calculated according to eq 22 to be 28%, in good agreement with the observed value of ca. 25%. This further supports the validity of the proposed mechanism and illustrates the predictive power of the kinetic analysis.

Temperature Dependence of the Rate of Catalytic Hydrogenation. Though not previously studied in great detail, it is known that temperature can strongly influence the enantioselectivity of asymmetric hydrogenation.[5] Because the activation enthalpies for the oxidative addition of H_2 to complexes of the type [Rh(diphosphine)(mac)]$^+$ are known to be lower than those for the catalyst–substrate adduct dissociation ($\Delta H^\ddagger$ = 13 kcal/mol for dissociation vs. $\Delta H^\ddagger$ = 8 kcal/mol for H_2 oxidative addition in the case of [Rh(diphos)(mac)]$^+$) competition of H_2 oxidative addition ($k_2[H_2]$) with dissociation (k_{-1}) will occur at lower H_2 pressures with decreasing reaction temperature. Since this competition is responsible for the lowering of the enantioselectivity with increasing H_2 pressure (by lowering the steady-state concentration of $\mathbf{2}^{min}$, the intermediate from which the major product is derived), it is predicted that the enantioselectivity will increase

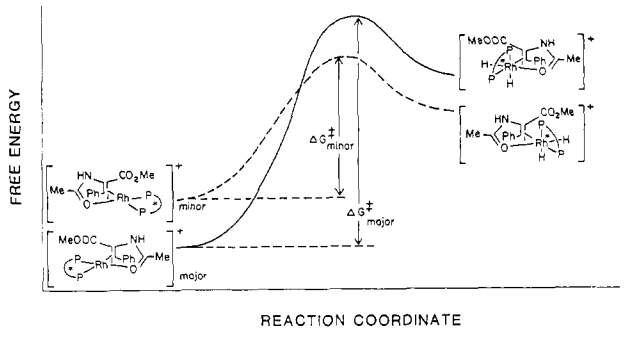

Figure 9. Schematic reaction coordinate profiles for the enantio-determining reactions of the diastereomeric [Rh(dipamp)(mac)]$^+$ adducts with H_2.

with increasing temperature and that increasing temperature will offset the detrimental effect of increasing the H_2 pressure. Confirmation of this expectation is provided by the data in Table V and Figure 8. At H_2 partial pressure at 5 atm, the enantioselectivities are observed to increase from 73% ee to values of 83% and 89% ee, as the temperature is increased from 0 °C to 14.8 and 37.0 °C, respectively. At each temperature the kinetic data are in excellent accord with eq 23 and 24. The rate constants and activation parameters obtained from these measurements are listed in Table VI. The enthalpies of activation for the enantio-determining step, the oxidative addition of H_2 to $\mathbf{2}^{maj}$ and $\mathbf{2}^{min}$, differ by 3.2 kcal/mol ($\Delta H^\ddagger$ = 10.7 for k_2^{maj} and 7.5 kcal/mol for k_2^{min}), accounting for most of the difference of transition-state energies between the two diastereomeric pathways. In the low-pressure (Curtin–Hammett) limit, it is the difference between these transition-state free energies that determines the enantioselectivity.

The unusual temperature and H_2 pressure dependencies of the asymmetric hydrogenation reaction have implications for the optimization of rate and enantioselectivity. It is attractive to run the asymmetric hydrogenation reaction at high H_2 pressure in order to obtain higher rates. The lowered enantioselectivities obtained at high H_2 pressures can be offset by higher temperatures. Fortunately, higher reaction temperatures have little influence on the enantioselectivity in the low-pressure limit (e.g., 96% ee is obtained at 37 °C in the low-pressure limit) and lead to higher rates in two ways: (1) by increasing the magnitude of all the rate constants and (2) by extending the low-pressure limit, where the reaction rate is first-order in H_2 pressure, to higher pressures.

These characteristic patterns of H_2 pressure and temperature dependencies of optical yields also have been observed for most of the other asymmetric hydrogenation catalysts examined thus far,[5,16] suggesting that the mechanism of enantioselection that has been demonstrated for this system is quite general for this class of catalysts.

Origin of Enantioselection. We have shown that the efficient enantioselection exhibited by this catalyst (up to 98% ee) is due to the markedly higher reactivity toward H_2 of the less stable catalyst–substrate adduct ($\mathbf{2}^{min}$) compared with the predominant one ($\mathbf{2}^{maj}$). The origin of this striking reactivity difference still is unclear. It is, of course, not unexpected that the less stable of a pair of diastereomers will exhibit the higher reactivity by virtue of its initially high free energy. However, to account for the enantioselectivity of the reaction, the difference in selectivity must be much greater than the difference in stability of the diastereomers, indeed at least 50 times greater to accommodate an optical yield of 96% ee. The 580-fold difference in the reactivity of the two diastereomers of [Rh(dipamp)(mac)]$^+$ corresponds to a $\Delta\Delta G^\ddagger$ of 3.7 kcal/mol [$\Delta\Delta H^\ddagger$ = 3.2 kcal/mol; $\Delta\Delta S^\ddagger$ = −2 cal/(mol K), Table VI]. This is made up of contributions of ΔG = 1.4 kcal/mol, representing the initial difference in free energy between the two diastereomeric adducts and ΔG = 2.3 kcal/mol representing the difference between the transition-state free energies. The limiting (i.e., low H_2 pressure–high temperature)

(15) Okrasinski, S. J.; Halpern, J., unpublished results.

(16) Knowles, W. S.; Sabacky, M. J.; Vineyard, B. D. *Adv. Chem. Ser.* **1974**, *132*, 274.

selectivity is determined solely by the latter difference.

It has been suggested[1a] that the reactivity difference between the two diastereomeric adducts has its origin in the stability difference of the products of the oxidative addition of H_2 (i.e., $[RhH_2(dipamp)(mac)]^+$]), the order of stabilities of these diastereomeric products being opposite to that of the parent catalyst–substrate adducts. The reaction profiles depicting this behavior, which is characterized by crossing of the two profiles, are depicted in Figure 9. In the sense of the "Hammond postulate" this corresponds to the reaction being under "product control."[17]

Since the behavior depicted in Figure 9 appears to be quite general for this class of asymmetric hydrogenation reactions (i.e., involving ligands and substrates),[5,16] its origin must reflect some systematic feature of the reactions. A plausible suggestion is that the reason for the inverted order of stabilities of the initial catalyst–substrate adducts and the dihydrides derived from them is the trans disposition of the substrate and diphosphine chelate rings in the former case and the cis disposition in the latter (Figure 9). Unfortunately, all attempts to intercept and examine the dihydride intermediates in these reactions, and thus to probe this theme directly, have thus far been unsuccessful. This failure is consistent with the endothermicity of the H_2 oxidative addition step that is a feature of the behavior depicted in Figure 9.

Acknowledgment. Support of this research through a grant from the National Science Foundation (CHE 82-17950) and a generous loan of rhodium from Johnson-Matthey Co. are gratefully acknowledged. The NMR facilities used in this research were supported in part through The University of Chicago Cancer Center Grant No. NIH-CA-14599.

Registry No. 1, 75397-16-9; 2^{maj}, 75109-58-9; 2^{min}, 75109-57-8; [Rh(DIPAMP)]$^+BF_4^-$, 106502-35-6; methyl (*Z*)-α-acetamidocinnamate, 60676-51-9; toluene, 108-88-3; silane, 7803-62-5.

(17) *Asymmetric Catalysis*; Bosnich, B., Ed. NATO ASI Series E, No. 103. Martinus Nijhoff: Dordrecht, 1986; pp 15–17.

Concerning the Mechanism of Formation of Oxygen Difluoride[1]

Evan H. Appelman* and Albert W. Jache[2]

Contribution from the Chemistry Division, Argonne National Laboratory, Argonne, Illinois 60439. *Received August 27, 1986*

Abstract: Passage of F_2 over ice at temperatures around −50 °C produces a mixture of O_2, HOF, and OF_2, along with small amounts of H_2O_2. The involvement of HOF in the formation of OF_2 has been demonstrated through the use of HOF labeled both with ^{18}O and with radioactive ^{18}F. The reaction that produces the OF_2 has been shown to be

$$F_2 + HOF \rightarrow OF_2 + HF$$

The OF_2 contains one fluorine atom from the F_2 and one from the HOF.

Oxygen difluoride was first synthesized by Lebeau and Damiens in 1927.[3] Although their initial method of preparation was electrochemical, they also observed that the compound was formed when fluorine was passed through aqueous alkali.[4] Cady, in his classic study of the reaction of fluorine with aqueous solutions, systematized our knowledge of the formation of OF_2.[5] He observed that it was formed to a negligible extent in water or acidic media and that its yield rose to a maximum of about 60% in 0.5–1 M alkali. Oxygen difluoride was subsequently observed to be formed when fluorine was passed through 60% $HClO_4$ in a graphite apparatus[6] or when it reacted with H_5IO_6.[7] A relatively recent study has shown that OF_2 can also be made in good yield by the reaction of fluorine with hydrated alkali fluorides.[8]

Despite this body of literature, there has been virtually no attempt made to elucidate the mechanism by which OF_2 is produced. If we think of the compound as the acid anhydride of HOF, its formation in dilute aqueous solutions seems particularly puzzling. In our previous study of the reaction of fluorine with aqueous media, we proposed a mechanism that accounted for the production of HF, HOF, H_2O_2, and O_2 but explicitly left open the question of OF_2 formation.[9] However, in the course of our studies of the production and utilization of hypofluorous acid, our attention was continually drawn to the fact that substantial amounts of OF_2 were always formed as a byproduct in the synthesis of HOF. We drew the tentative conclusion that HOF was probably involved in the production of OF_2, and we even suggested the thermodynamically plausible reaction[9]

$$F_2 + HOF \rightarrow OF_2 + HF \quad (1)$$

In the present paper, we have undertaken to verify the involvement of HOF in the production of OF_2 and to attempt to shed some light on the overall mechanism of the reaction.

Experimental Section

Reagents. Fluorine was a standard industrial product (Matheson Co, minimum purity 98%). When necessary, it was freed of HF by passage through traps cooled with liquid nitrogen or liquid oxygen. Nitrogen used to transfer HOF was Airco "prepurified" grade. Water enriched in oxygen-18 (nominal 99 atom %) was obtained from Norsk Hydro, Oslo. Other chemicals were commercial products of analytical reagent grade.

Reaction of Fluorine with Ice. The apparatus used to carry out reactions of fluorine with cold ice is shown in Figure 1. Of the plastic U-tube traps, trap B was the reaction vessel, trap A served to collect OF_2, traps C and D removed water and much of the HF, trap E collected HOF, and trap F protected trap E from impurities that might be evolved by the circulating pump G. The metal vacuum line served both to complete the circulation loop and as a reservoir for fluorine. By varying the number of segments of this line that were included in the loop, the

(1) Work supported by the U.S. Department of Energy, Division of Chemical Sciences, under Contract W-31-109-Eng-38.

(2) Present address, Department of Chemistry, Marquette University, Milwaukee, WI 53233.

(3) Lebeau, P.; Damiens, A. *C.R. Hebd. Seances Acad. Sci.* **1927**, *185*, 652.

(4) Lebeau, P.; Damiens, A. *C.R. Hebd. Seances Acad. Sci.* **1929**, *188*, 1253.

(5) Cady, G. H. *J. Am. Chem. Soc.* **1935**, *57*, 246.

(6) Rohrback, G. H.; Cady, G. H. *J. Am. Chem. Soc.* **1947**, *69*, 677.

(7) Rohrback, G. H.; Cady, G. H. *J. Am. Chem. Soc.* **1948**, *70*, 2603.

(8) Borning, A. H.; Pullen, K. E. *Inorg. Chem.* **1969**, *8*, 1791.

(9) Appelman, E. H.; Thompson, R. C. *J. Am. Chem. Soc.* **1984**, *106*, 4167.

0002-7863/87/1509-1754$01.50/0